CFD BASED HEAT TRANSFER ANALYSIS OF SOLAR AIR HEATER DUCT PROVIDED WITH ARTIFICIAL ROUGHNESS

Vivek Rao, Dr. Ajay Gupta, Amit Kumar

Abstract- In the present study, the thermo-hydraulic performance of four ribs–roughened rectangular duct is investigated. The aspect ratio of the duct was kept constant as 5. Symmetry and periodic boundary conditions are used to minimize the computational cost. Four rib configurations were tested: V-up rib, V-up Broken rib, V-down broken rib, and Multi V rib pointing upstream of the main flow direction. Profile boundary condition was created at the outlet of the test section and was applied to various inlet conditions of main rib configuration. For all cases hydraulic diameter and angle of attack were kept constant to 33 mm and 600. Only relative roughness pitch and Reynolds number were varied from 8-12 and 8000-15000.

CFD simulation software, ANSYS (workbench mode) has been used for simulation. Fluid flow (FLUENT) module has been used to demonstrate detailed temperature distribution, velocity path-line between a pair of ribs on the ribbed surface. The secondary flow and vortices' caused by the inclination of the rib and broken condition of rib create a significant span wise variation of heat transfer coefficient due to turbulent associated with it. Y plus value is calculated to test the accuracy of the mesh. Solar air heater provided with Multi-V rib gives maximum Nusselt number of 145 at relative roughness pitch of 8 and Reynolds number of 15000.

Keyword: CFD simulation, Solar air heater, Symmetric and Periodic rib, artificial roughness, vortices

1 INTRODUCTION

The primary forms of solar energy are heat and light. In recent years solar energy has been strongly promoted as a viable energy source. One of the simplest and most direct applications of this energy is the conversion of solar radiation into heat [1]. Purpose of solar air heater is to convert the solar radiation into heat to satisfy energy needs but with some limitations it is not being used on grid scale because of its poor efficiency and higher initial cost. So there is a requirement of advancement in the flat plate collector to overcome its limitations so that it can be used as a replacement of conventional heaters and electric power consuming devices.

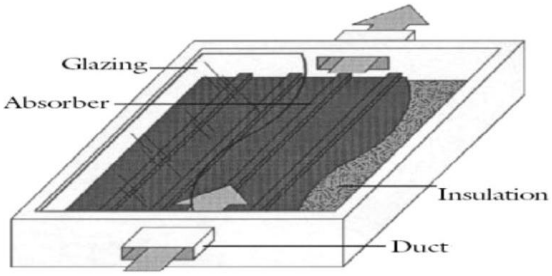

Fig.1. Flat Plate Collector [1]

- *VivekRao is Assistant Professor in Mechanical Engineering Department in Subharti University Meerut, U.P, India, PH-09639011202. E-mail:vivekrao99@gmail.com.*
- *Dr. Ajay Gupta is Associate professorin Industrial and Production Engineering Department in National Institute of Technology Jalandhar, India. E-mail: guptaa@nitj.ac.in*
- *Amit Kumar is Assistant Professor in Mechanical Engineering Department in Subharti University Meerut, U.P, India, PH-09639011202. E-mail:amitnitj1@gmail.com.*

The term 'flat plate' is slightly misleading in the sense that surface may not be truly flat it may be a combination of flat, grooved or of other shapes as the absorbing surface with some kind of heat removal device like tubes or channels. A flat-plate solar collector as shown in Fig. 1 consists of a water proof, metal or fiberglass insulated box containing a dark colored absorber plate, with one or more translucent glazing. The glazing covers reduce the convection and radiation heat losses to the environment.

Thermal performance may be increased by increasing convective heat transfer coefficient. There are two way for increasing heat transfer coefficient either increase the area of absorbing surface by using fins or create the turbulence on the heat transferring surfaces.

Artificial roughness is basically a transfer enhancement technique by which thermo hydraulic performance of a solar air heater can be improved. The thermal efficiency of solar air heater is generally poor due to low heat transfer co-efficient between the absorber plate and the air flowing in to the duct due to the formation of laminar sub layer on the absorber plate which acts as heat transferring surface [6]. So there is a need to break the laminar sub layer therefore, artificial roughness has been used extensively for the enhancement of forced convective heat transfer, which further requires flow at the heat-transferring surface to be turbulent. However, energy for creating such turbulence has to come from the fan or blower and the excessive power is required to

flow air through the duct. Therefore, it is desirable that the turbulence must be created only in the region very close to the heat transferring surface, so that the power requirement may be reduced.

The overall objective of this study was to investigate the effect of various dimensionless parameter on physics of heat transfer process in terms of Nusselt number using FEM simulations. The specific tasks were to:

1. To analyze the performance (in terms of Nusselt number) of artificially roughened solar duct by varying the relative roughness pitch and Reynolds number.
2. To compare the performance of different roughness geometries.
3. Draw the various graph like flow distribution, pathline, temperature contour and Reynolds number vs. Nusselt number and simulate the total heat transfer on absorber plate by CFD technique

2 THE SOLAR BOX SIMULATION SETUP

The cross sectional dimension of the duct considered for this analysis are 100mm x 20mm respectively as shown in Fig. 2. The aspect ratio has been kept 5 for this analysis. The flow system consists of 166.6mm long inlet test section and a constant heat flux of 1000W/m² is applied on the absorber plate. The inlet test condition of solar air heater is same for all the roughness's under investigation.

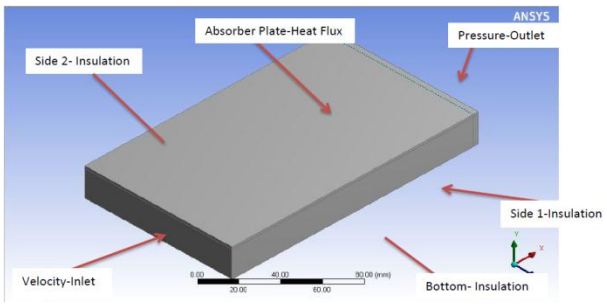

Fig.2. Geometric model (test section)

2.1 Concept of periodic and symmetric rib [2]

It is observed that in most of the cases nature of rib in solar air heater is periodic and also some of them are symmetric. Separate inlet test section domain is created of the same boundary condition and velocity profile created at outlet section for different Reynolds no. is used as inlet velocity condition for the periodic and symmetric domain condition.

Therefore in present work periodic and symmetric domain is used as shown in Fig. 3. to minimize cost and time.

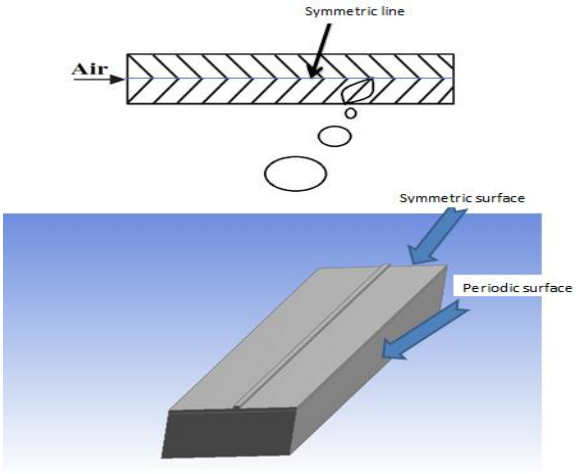

Fig.3. Symmetric and periodic rib

Theperiodic and symmetric type of geometry is taken for solar air heater and the thickness of absorber plate is same as inlet test section

3. CFD SIMULATION [3]

FEM simulation software, ANSYS version 14.5 (workbench mode) has been used forsimulation. Fluid flow (FLUENT) module has been used in present work. Fluid flow (FLUENT) module predicts the outlet temperature, velocity, flow behavior to great accuracy due to application of thermal loading on the work piece. Different types of thermal loading that can be applied on the work piece in Fluid flow (FLUENT) module are temperature, convection, radiation and heat flux.

3.1 Formulation of the CFD Model [5]

In Reynolds averaging, the solution variables in the instantaneous (exact) Navier- Stokes equations are decomposed into the mean (ensemble-averaged or time-averaged) and fluctuating components. For the velocity components:

$$u_i = \bar{u}_i + u_i' \quad (1)$$

Where $\acute{u}_i$ and u_i' are the mean and fluctuating velocity components (i = 1, 2, 3). Likewise, for pressure and other scalar quantities:

$$\emptyset = \bar{\emptyset} + \emptyset' \quad (2)$$

Where $\emptyset$ denotes a scalar such as pressure, energy, or species concentration. Substituting expressions of this form for the flow variables into the instantaneous continuity and momentum equations and taking a time (or ensemble) average (and dropping the over bar on the mean velocity) yields the ensemble-averaged momentum

equations. They can be written in Cartesian tensor form as:

$$\frac{\partial \rho}{\partial t} + \frac{\partial}{\partial x_i}(\rho u_i) = 0 \quad (3)$$

$$\frac{\partial}{\partial t}(\rho u_I) + \frac{\partial}{\partial x_j}\left(\rho u_i u_j\right) = -\frac{\partial p}{\partial x_i} + \frac{\partial}{\partial x_i}\left[\mu\left(\frac{\partial u_i}{\partial x_j} + \frac{\partial u_j}{\partial x_i} - \frac{2}{3}\delta_{ij}\frac{\partial u_i}{\partial x_j}\right)\right] + \frac{\partial}{\partial x_j}\left(-\rho\overline{u'_i u'_j}\right) \quad (4)$$

Equations 3 and 4 are called Reynolds-averaged Navier-Stokes (RANS) equations. They have the same general form as the instantaneous Navier-Stokes equations, with the velocities and other solution variables now representing ensemble-averaged (or time-averaged) values. Additional terms now appear that represent the effects of turbulence. These Reynolds stresses, $-\rho\overline{u'_i u'_j}$, must be modeled in order to close equation.

For flows with heat transfer, FLUENT solves conservation equation for mass, momentum and energy. For flows involving species mixing or reactions, a species conservation equation can be used.

The shear-stress transport (SST) k-ω model was developed by Menter [4] to effectively blend the robust and accurate formulation of the k-ω model in the near-wall region with the free-stream independence of the k- model in the far field. To achieve this, the k- model is converted into a k-ω formulation.

$$\frac{\partial}{\partial x}(\rho k) + \frac{\partial}{\partial x_i}(\rho k u_i) = \frac{\partial}{\partial x_j}\left(\tau_k \frac{\partial K}{\partial x_j}\right) + G_{k+} G_b - \rho_\varepsilon - Y_M + S_k \quad (5)$$

$$\frac{\partial}{\partial t}(\rho\varepsilon) + \frac{\partial}{\partial x_i}(\rho\varepsilon u_i) = \frac{\partial}{\partial x_j}\left(\tau_k \frac{\partial \omega}{\partial x_j}\right) + c_{1\varepsilon}\frac{\varepsilon}{k}(G_k + c_{3\varepsilon}G_b) - c_{2\varepsilon}\rho\frac{\varepsilon^2}{K} - R_\varepsilon + S_\varepsilon \quad (6)$$

In these equations, G_k represents the generation of turbulence kinetic energy due to mean velocity gradients. G_ω represents the generation of ω. τ_k and τ_ω represent the effective diffusivity of k and ω, respectively. Y_k and Y_ω represent the dissipation of k and ω due to turbulence.

Mass Conservation equation

$$\frac{\partial}{\partial x}(\rho u) + \frac{\partial}{\partial x}(\rho v) = 0 \quad (7)$$

Momentum Conservation

$$\rho\left(\mu\frac{\partial u}{\partial x} + v\frac{\partial u}{\partial y}\right) = g(\rho_\infty - \rho) + \frac{\partial}{\partial y}\left(\mu\frac{\partial u}{\partial y}\right) \quad (8)$$

Energy equation

$$\rho c_p\left(\mu\frac{\partial t}{\partial x} + v\frac{\partial t}{\partial y}\right) = \frac{\partial}{\partial x}\left(k\frac{\partial t}{\partial y}\right) \quad (9)$$

3.2 SST k ω MODEL

The shear-stress transport (SST) k-ω model was developed by Menter [4] to effectively blend the robust and accurate formulation of the k-ω model in the near-wall region with the free-stream independence of the k- model in the far field. To achieve this, the k- model is converted into a k-ω formulation.

$$\frac{\partial}{\partial t}(\rho k) + \frac{\partial}{\partial x_i}(\rho k u_i) = \frac{\partial}{\partial x_j}\left(\tau_k \frac{\partial K}{\partial x_j}\right) + G_k - Y_k + S_k \quad (10)$$

$$\frac{\partial}{\partial t}(\rho\omega) + \frac{\partial}{\partial x_i}(\rho\omega u_i) = \frac{\partial}{\partial x_j}\left(\tau_k \frac{\partial \omega}{\partial x_j}\right) + G_\omega - Y_\omega + S_\omega \quad (11)$$

In these equations, G_k represents the generation of turbulence kinetic energy due to mean velocity gradients. G_ω represents the generation of ω. Γk and Γω represent the effective diffusivity of k and ω, respectively. Y_k and Y_ω represent the dissipation of k and ω due to turbulence.

3.3 Simulation Setup

MESHING: Tetrahedral (Patch independent) mesh method is used as shown in Fig. 5 and 6. Table 1 gives the mesh detail.

Table 1. Mesh characteristics (test section)

Type of element	Tetrahedral
Number of nodes	302564
Number of elements	941451

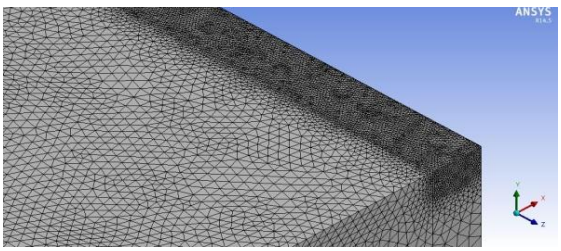

Fig.5. Mesh Details (Test Section)

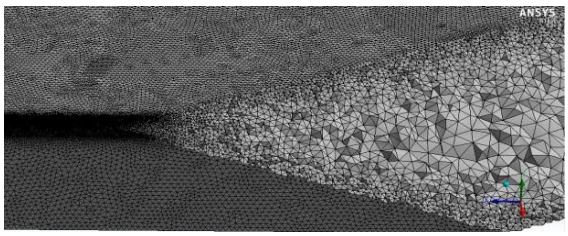

Fig.6. Interior Mesh Details (Test Section)

Boundary Conditions: To analyze the flow and heat transfer 3-D model has been set up instead of 2-D model for the selected geometry because secondary flow takes place. Shear Stress Transport (SST) k - w with turbulence intensity (5%) is used because SST model is more accurate to experimental value. To control the radiation intensity & direction a discrete ordination (DO) irradiation model is used & also employs the energy equation. The various boundary conditions employed are given in table 2

Table 2. Boundary conditions for all cases of rib

Location	Boundary Type	Boundary Details		
Air inlet	Velocity Inlet	Velocity	Reynolds Number	Turbulent Intensity
		2.3366	8000	5.2027
		3.5049	12000	4.9456
		4.3812	15000	4.8095
Outlet	Pressure Outlet	Gauge Pressure 0		
Side 1, Side2 & Bottom	Wall	No slip wall		
		Adiabatic with no heat loss		
		Material used - Wood.		
Absorber Plate	Wall	Heat Flux – 1000W/m^2		
		Material used – Aluminum		
		Emissivity -1.0		
		Density-2719 kg/m^3		
		Thermal Conductivity -202.4 W/m/C		

4. Result and Discussion

4.1. Grid Independence Test

A grid-dependency study is carried out to evaluate mesh suitability for the turbulent flow through the artificially roughened solar air heater. A grid independence test is implemented over grids with different numbers of Nodes 176391, 302564, and 419985 that are used in three steps and tabulated in table 3. It is found that the variation in Nusselt number and friction factor is marginal increase when moving from 384678 cells to 429413. Hence, there is no such advantage in increasing the number of cells beyond this value. Thus, the grid system of 384678 cells is adopted for the current computation.

Table 3. Grid independence test

Mesh size	Nodes	% difference in Nusselt number
0.25 mm	17639	----
0.15 mm	302564	2.79
0.13 mm	419985	0.449

4.2 Selection of Model

No universal turbulence model exists that caters for all ranges of flow, laminar or turbulent. The choice of turbulence model is not only dictated by the type of flow but also by the availability of computational power and the accuracy desired.
Values of Nusselt number at different Reynolds number for different models are shown in Fig. 7.

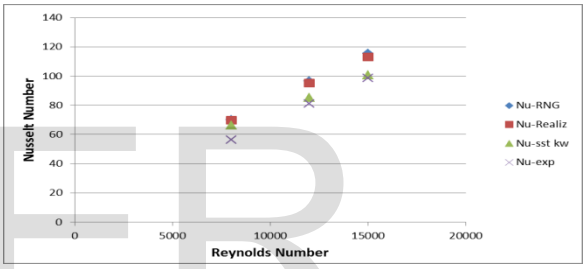

Fig.7. Nusselt Number Vs. Reynolds Number (test section)

To select the turbulence model, the previous experimental study is simulated using different low Reynolds number models such as Standard k-ω model, Renormalization-group k-ε model, Realizable k-ε model and Shear stress transport k-ω model for fix values of relative roughness pitch (p/e) of 8 and relative roughness height (e/D) of 0.03. The results of different models are compared with experimental results. The Shear stress transport k-ω model was selected on the basis of its closer results to the experimental results

4.3 V-up Ribs

Theperiodic and symmetric type of geometry is taken for solar air heater and the thickness of absorber plate is same as inlet test section i.e. 3 mm. Roughness in the form of V-up ribs created on the underside of the absorber plate while remaining three sides are consider smooth surfaces as shown in Fig. 8. The material for absorber plate is aluminium and the ranges of parameter are predicted as shown in table 4.

Table 4. Range of parameter for all configurations of ribs

Reynolds number (Re)	8000, 12000, & 15000
Relative roughness pitch (p/e)	8, 10, & 12
Relative roughness height ($e/D_{H)}$	1
Angle of attack (α)	600

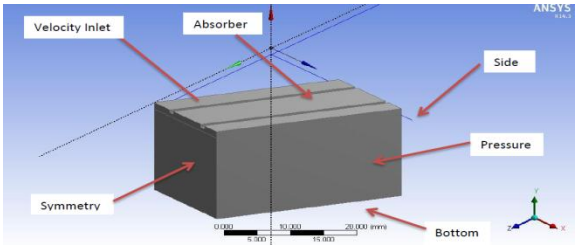

Fig.8. Geometric model (V-up shapedRibs)

Mesh size is increases with increase in dimension of domain, for different value of Relative roughness pitch number of nodes and element size is varies. With the consideration of periodic and symmetric condition the prediction of result is more accurate as the number of node or mesh size is enough for this condition

Fig.9. shows the variations of Nusselt number with Reynolds number for different value of relative roughness pitch. The values of maximum Nusselt number are found to be 111.178 atpitch 8 and Reynolds number 15000, also Nu no. is increase with increase in value of Reynolds number in all cases; it may be due to the turbulence associated with higher velocity.

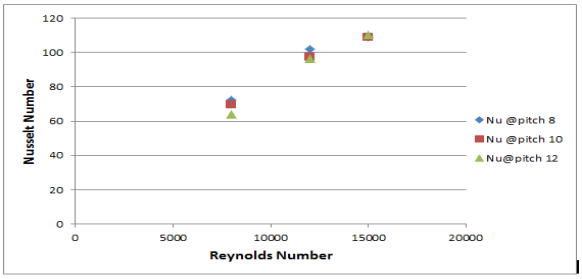

Fig.9. Nusselt number Vs. Reynolds number for V-up rib

The temperature distribution is the consequence of the combination of convection and conduction. Convection takes away heat from the local position i.e. from the absorber plate while conduction tends to equalize the wall temperature distribution.

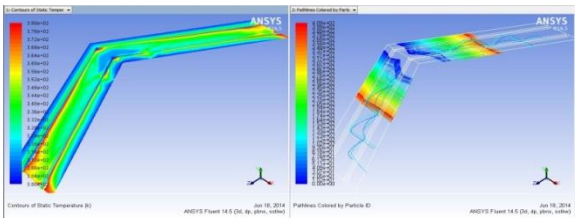

Fig.10. Temperature contour and pathline at Reynolds number 8000 (V-up rib)

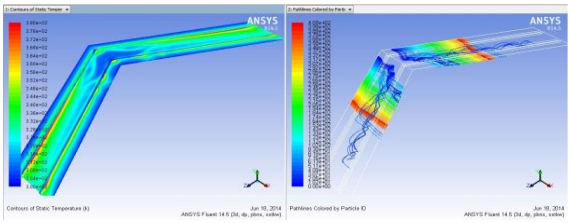

Fig.11. Temperature contour and pathline at Reynolds number 12000 (V-up rib)

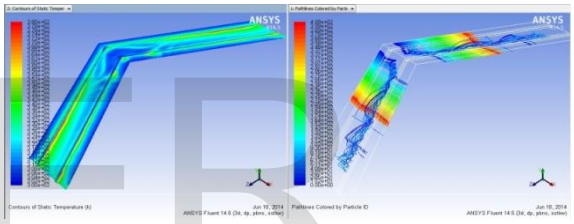

Fig.12. Temperature contour and pathline at Reynolds number 15000 (V-up rib)

The central area has less heat transfer coefficient due to the divergence of flow by the rib. As shown in Fig. 10, 11 and 12 heat transfer coefficient increases as move away from the center because of high fluid velocity. While in the corner regions unheated side and bottom wall forces the temperature to decreases

Due to presence of rib pointing in the upward direction, secondary flow and vortices' are induces and because of this, intensity of the turbulence is increases which leads to higher heat transfer rate. The moving vortices' carry warmer air towards the side end of solar air heater illustrated in the Fig.12. The secondary flow can be altered by the confinement of the walls in the ducts such as square ones. The wall aspect ratio reduces the regions where the secondary flows are directed towards V-ribs pointing upstream and downstream.

CFD results have critically analyzed the flow separation and reattachment to explain other

related phenomenon such as increase in Nusselt number for different roughness parameters.

It is also seen that Nusselt number values increase with the increase in relative roughness height for fixed value of relative roughness pitch. The maximum value of Nusselt number occurs at a relative roughness pitch of 8 at a Reynolds number of 12,000.

Vortices, separation of flow andreattachment have been predicted by CFD model. For a fixed value of relative angle of attack (60^0) and relative roughness height number of vortices, intensity and reattachment point varies with respect to the Reynolds number.

4.4 V-up broken rib

Fig. 13 shows the variation of Nusselt number with Reynolds number with varying relative roughness pitch for a given value of relative roughness height. The values of Nusselt number are found to increase with increasing value of Reynolds number in all cases. The maximum value of Nusselt number occurs at relative roughness height 1mm at a Reynolds number 15000 and relative roughness pitch 8. The maximum value of Nusselt number is 112.883.

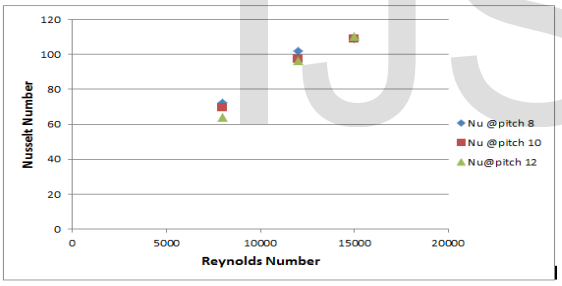

Fig.13. Nusselt number Vs. Reynolds number for V-up broken rib

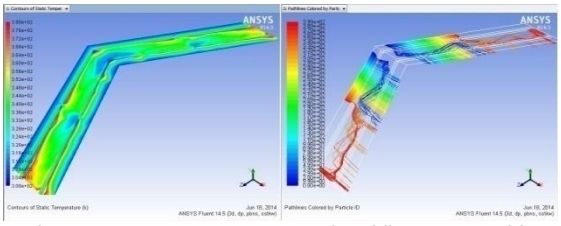

Fig.14. Temperature contour and pathline at Reynolds number 8000 (V-up broken rib)

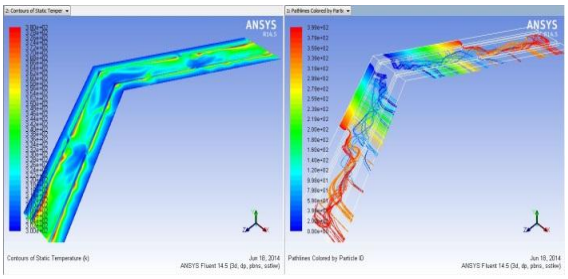

Fig.15. Temperature contour and pathline at Reynolds number 12000 (V-up broken rib)

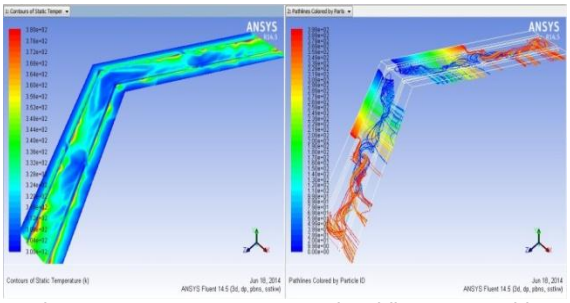

Fig.16. Temperature contour and pathline at Reynolds number 15000 (V-up broken rib)

In this case Nusselt number is found at relative roughness pitch 8, therefore comparison is shown at pitch 8 and different Reynolds number. Temperature contours and path-line is shown in Fig. 14, 15 and 16. From the Fig. 16, it is clear that large secondary flow and more vortices are occur at Reynolds number 15000 as expected due to turbulence associated with it.

4.5 V-down broken rib

Fig. 17 shows the variation of Nusselt number with Reynolds number with varying relative roughness pitch and Reynolds number for a given value of relative roughness height. The values of Nusselt number are found to increase with increasing value of Reynolds number in all cases. The maximum value of Nusselt number occurs at relative roughness height 1mm at a Reynolds number 15000 and relative roughness pitch 8. The maximum value of Nusselt number is found to be 117.244.

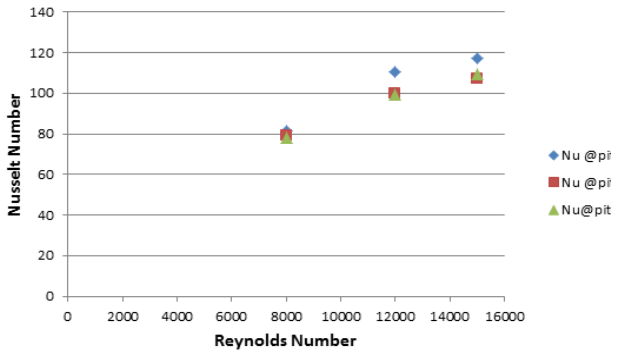

Fig.17. Nusselt number Vs. Reynolds number for V-down broken rib

As maximum value of Nusselt number is found at relative roughness pitch 8, therefore comparison is shown at pitch 8 and different Reynolds number. From the Fig. 4.16 it is clear that large secondary flow and more vortices are occur at Reynolds number 15000 as expected due to turbulence associated with it.

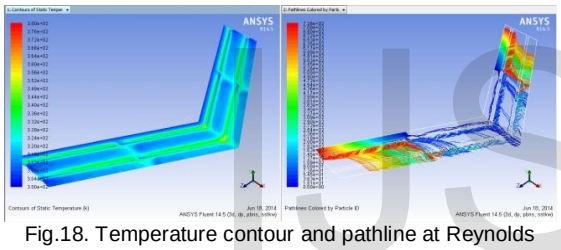

Fig.18. Temperature contour and pathline at Reynolds number 8000 (V-down Broken rib)

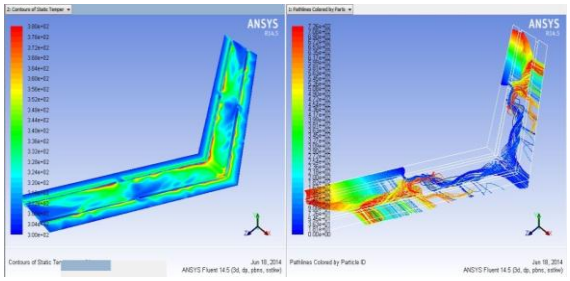

Fig.19. Temperature contour and pathline at Reynolds number 12000 (V-down broken rib)

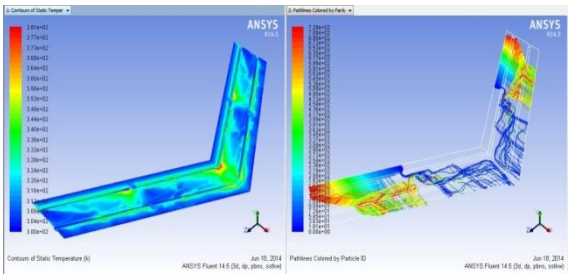

Fig.20. Temperature contour and pathline at Reynolds number 12000 (V-down broken rib)

As maximum value of Nusselt number is found at relative roughness pitch 8, therefore comparison is shown at pitch 8 and different Reynolds number as shown in Fig. 18, 19 and 20. From the Fig. 20 it is clear that large secondary flow and more vortices' are occur at Reynolds number 15000 as expected due to turbulence associated with it.

4.6 Multi V rib rib

Fig. 21 shows the variation of Nusselt number with Reynolds number with varying relative roughness pitch for a given value of relative roughness height. The values of Nusselt number are found to increase with increasing value of Reynolds number in all cases. The maximum value of Nusselt number occurs at relative roughness height 1mm at a Reynolds number 15000 and relative roughness pitch 8. The maximum value of Nusselt number is 143.885

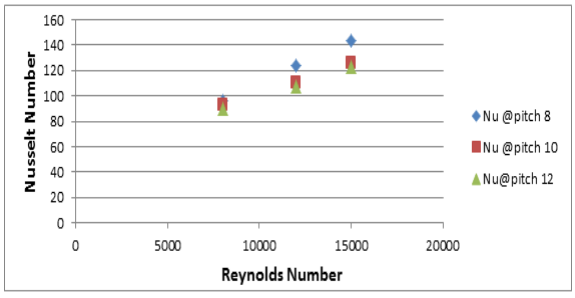

Fig. 21 Nusselt number Vs. Reynolds number for Multi V rib

There are 10 small V rib in Multi v rib in this configuration, each part of the V-rib independently introduces its own secondary flow and vortices', resulting in high turbulence and thus high heat transfer coefficient. But the main disadvantage in this case is the pressure drop is substantial.

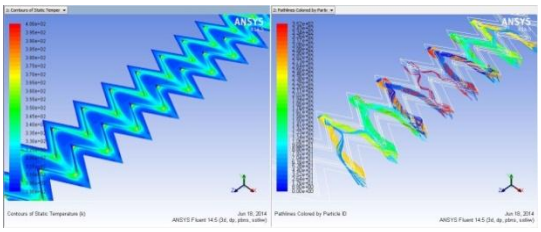

Fig. 22 Temperature contour and pathline at Reynolds number 12000 (Multi V rib)

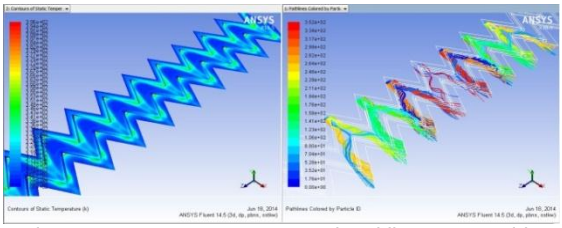

Fig. 23. Temperature contour and pathline at Reynolds number 12000 (Multi V rib)

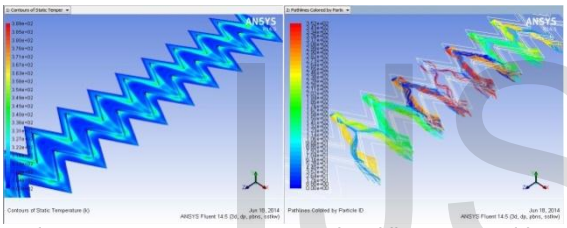

Fig. 24. Temperature contour and pathline at Reynolds number 15000 (Multi V rib)

As maximum value of Nusselt number is found at relative roughness pitch 8, therefore comparison is shown at pitch 8 and different Reynolds number as shown in Fig. 22, 23 and 24. From the Fig. 24 it is clear that large secondary flow and more vortices' are occur at Reynolds number 15000 as expected due to turbulence associated with it

5. CONCLUSION AND FUTURE SCOPE

This simulation module predicts the velocity path-line and the temperature contour to predict the nature of flow of fluid and distribution and following conclusions were drawn:

1. There is a significant improvement in effective efficiency of solar air heater by providing different types of roughness elements on the absorber plate.
2. In the medium range of Reynolds number, Multi V ribs resulted in higher Nusselt number of 143.885 at relative roughness height (0.03), relative roughness pitch 8 and Reynolds number 15000 with medium range of pressure drop 2.2825 Pa.
3. Secondary flow and vortices' substantially increases the heat transfer rate, which is more effective in V-down broken rib after Multi V rib.
4. Heat transfer distribution depends upon type of dimensionless parameter and highest at a specific value,
5. Computational cost is saved by use of periodic and symmetry boundary condition.

REFERENCES

1. http://www.pasolar.ncat.org/lesson02.php.

2. Momin AME, Saini JS, Solanki SC. Heat transfer and friction in solar air heater duct with V-shaped rib roughness on absorber plate. Int J Heat Mass Transf 2002, vol. 45, pp. 3383–96.

3. ANSYS FLUENT 14.5 Theory Guide. ANSYS, Inc.(2009).

4. Momin AME, Saini JS, Solanki SC. Heat transfer and friction in solar air heater duct with V-shaped rib roughness on absorber plate. Int J Heat Mass Transf 2002, vol. 45, pp. 3383–96.

5. ANSYS FLUENT 14.5 Theory Guide. ANSYS, Inc.(2009).

6. Varun, Saini R.P., Singal S.K., "Investigation on thermal performance of solar air heaters having roughness elements as a combination of inclined and transverse rib on the absorber plate", Renewable Energy, 2008, vol.33, pp.1398-1405.